Periodic forcing of a Brownian particle

Luc P. Faucheux, Gustavo Stolovitzky, and Albert Libchaber*
Center for Studies in Physics and Biology, Rockefeller University, 1230 York Avenue, New York, New York 10021
(Received 28 October 1994; revised manuscript received 17 February 1995)

We study the effect on a Brownian particle (2 μm diameter polystyrene sphere in water) of an infrared optical tweezer moving in a circle. For a given potential depth of the optical trap, three different regimes for the particle motion are observed as a function of the trap velocity. For small velocity of the tweezer (typically < 100 μm/s), the particle is trapped and moves with the beam. For intermediate velocities (between 100 μm/s and 3 mm/s), the particle escapes but is caught by the returning trap: its mean angular velocity scales asymptotically as the inverse of the trap rotation frequency. For large tweezer velocities (> 3 mm/s), the particle diffuses along the circle but is confined in the radial direction. We describe these observations by a simple deterministic model. We justify the use of this model solving the corresponding Fokker-Planck equation.

PACS number(s): 05.40.+j

I. INTRODUCTION

Focusing a laser beam creates an inhomogeneous intensity profile. This attracts a small dielectric particle near the beam focal point (region of highest intensity), as shown in Fig. 1. The trapping force for a 2 μm diameter polystyrene sphere in water is of the order of 1 pN [1,2]. As one moves this optical trap, the viscous drag (Stokes force), proportional to the particle velocity, will eventually cause the particle to escape from the trap. This happens in our experiment for a critical trap velocity of the order of 100 μm/s. The question we address in this paper is the following: What happens to a Brownian particle subjected to an optical trap moving faster than the critical velocity? In particular, does one still induce particle motion, or is the particle free to diffuse? To answer these questions we chose to study the particle response when moving the trap along a 12.4 μm diameter circle. In this geometry, the trap always returns before the particle diffuses away. It confines the particle motion to the circle. The particle angular displacement over a long time period is easily recorded, and is the main observation of our paper.

Three regimes are observed as a function of the trap velocity. For small velocities (below 100 μm/s), the viscous drag is smaller than the maximum trapping force: the particle is trapped and follows the beam. For velocities between 100 μm/s and 3 mm/s, the trapping force does not overcome anymore the viscous drag and the particle escapes. However, it does not have enough time to diffuse away before the trap returns and kicks it for a brief instant. The mean particle angular velocity scales asymptotically as the inverse of the trap rotation frequency. Finally for velocities above 3 mm/s, the effect of the trap is smaller than the thermal noise, and no net drift of the particle is observed on time scales of the order of 2 min. The particle diffuses freely, *still confined in one dimension* along the circle. To summarize, the system evolves from a synchronous rotor to an asynchronous one, and finally to a free diffusive motion, always localized on the circle.

We present a theoretical treatment of the problem. Assuming the particle motion to be one dimensional, we study the response of a Brownian particle to a periodic forcing by a potential of arbitrary shape. Solving the equations of motion in the deterministic limit, where the stochastic term is assumed to be negligible, we recover the observed behavior for the *mean* particle angular frequency and for the *mean* residence time inside the trap. This is a surprising result considering the highly erratic

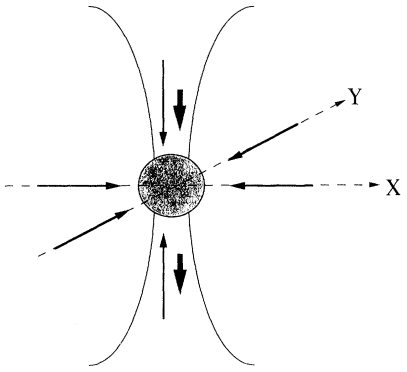

FIG. 1. A 2 μm diameter polystyrene particle trapped near the focal point of a Gaussian laser beam propagating down the vertical axis. The gradient forces are shown on each axis as the thin solid arrows. The radiation pressure is indicated by the thick solid arrows.

*Also at NEC Research Institute, 4 Independence Way, Princeton, NJ 08544.

 ©1995 The American Physical Society

appearance of the actual particle trajectories. Solving the Fokker-Planck equation, we study the effect of temperature and potential depth on the particle's motion. We justify the use of a zero temperature (deterministic) approach.

The paper is organized as follows. In Sec. II, we describe the optical tweezing technique and measure the profile of the trap. The trap is kept fixed in space. In Sec. III, we move the beam along a circle and record the angular displacement of the particle. We discuss the three regimes previously described. In Sec. IV, we present the deterministic and Fokker-Planck equations for this problem. We compare their predictions with the experimental results.

II. FIXED OPTICAL TRAP

We first present the sample preparation and the optical setup. We then describe the measurements on a fixed optical trap. Moving the microscope stage, we measure the maximum trapping force. Watching a particle fall into the trap, we extract the potential profile.

A. Experimental setup

Commercial suspensions of 2 μm diameter polystyrene spheres [3] are diluted in pure water [4]. The final volume fraction (10^{-4}) is such that hydrodynamic interactions are negligible. Typically only a few beads are seen in the microscope field of view (50×50 μm^2). Mylar sheets, 50 μm thickness, are cut and used as spacers between a microscope slide [5] and a coverslip [6]. Glassware are cleaned and dried using a nitrogen ionizing gun [7]. The cells are then filled with a suspension of spheres and sealed with fast epoxy [8] to avoid any convective flow. The sample, placed on the translation stage of an upright microscope [9], is observed under bright-field illumination. The particles tend to stay confined close to the bottom glass plate because of the gravitational field g. An estimate of this sedimentation effect is the Boltzmann length scale: $L_B = k_B T/\Delta m g$, where Δm is the relative mass of the particle. L_B is the average vertical excursion of the particle caused by thermal fluctuations. It is of the order of 2 μm. The vertical density of particles within the sample is then exponentially peaked within the first 2 μm close to the bottom plate. The image is recorded by a charge coupled device (CCD) camera [10]. The particle appears dark on a clear background. The video signal is processed in real time via a video board [11]. The pixel intensity is thresholded around the mean image value. From computing the center of gravity of the intensity distribution, the X and Y coordinates of the center of mass of the particle are deduced. The sampling rate is the video acquisition rate 30 Hz. The spatial resolution is 0.1 μm. The Z coordinate is not recorded: the particle never gets out of focus when running the experiment.

B. Optical trap

The TEM_{00} mode of a neodymium-doped yttrium aluminum garnet (Nd:YAG) laser [12] (wavelength = 1064 nm) is inserted into the microscope's optical path via the beam splitter B shown in Fig. 5. An $100\times$ oil immersed objective (OBJ) [13] focuses the beam to a sharp focal point inside the sample. The refractive index of the polystyrene sphere is larger than the water index; the particle is thus attracted to high electric field regions. The transverse Gaussian profile of the beam pulls the particle towards the beam axis. The converging beam develops a field gradient along its axis which opposes the radiation pressure. The forces acting on the sphere are shown in Fig. 1. The gradient forces localize the particle to the focal point, and the radiation pressure pushes the particle along the beam axis. When the gradient forces overcome the radiation pressure, the beam focal point becomes a trap, an optical tweezer, for the polystyrene sphere. This requires a microscope objective with a high enough numerical aperture, 1.3 in our case. The strength of the trap depends linearly on the output laser power. Because of optical losses due to reflections from the lenses and beam splitters along the optical path, the laser power at the level of the sample is 15 times smaller than the laser output.

We measure the maximum trapping force by moving the sample in a direction transverse to the optical axis. The particle escapes when the sample velocity is such that the Stokes force exceeds the trapping force. The critical velocity V_C as a function of the output laser power is shown in Fig. 2. The maximum trapping force is $6\pi\eta a V_C$, where η is the room temperature water viscosity (10^{-3} kg/m s) and a the particle radius. The value of the force is of the order of 1 pN for an output laser power of 150 mW. Taking 1 μm as a typical length, the trapping potential is then of the order of $300 k_B T$. The maximum trapping force depends critically on the position of the beam focal point with respect to the bottom glass plate. This is due to the laser reflection from the water-glass interface, which reduces the overall radiation pressure on the particle. Shifting upward the vertical position of the beam focal point by less than 5 μm decreases the maximum trapping force by a factor of 5. When running the experiment, we constantly check the distance between the beam focal point and the glass plate by imaging the laser reflection from the glass plate, and

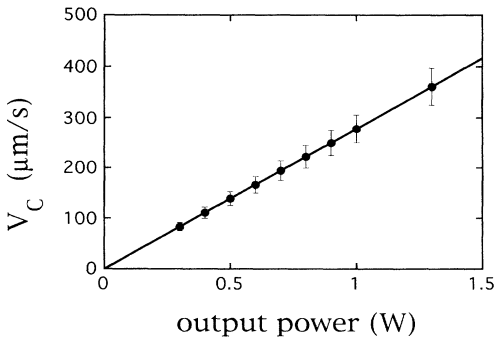

FIG. 2. The critical velocity V_C as a function of the output laser power.

adjust it to within 0.1 μm.

Another measure of the potential is obtained by observing the fall of a particle into the trap [14] for an output laser power of 150 mW (laser power at the level of the sample of the order of 10 mW). Figure 3(a) shows the time series of the particle position, when initially close to the trap. The trap is fixed and defines the axis origin. When random diffusion brings the particle to within a few micrometers of the trap, the particle is attracted and falls into it. The equation of motion for the particle is

$$m\frac{d}{dt}\vec{V}_P = -6\pi\eta a\vec{V}_P - \vec{\nabla}U + \vec{f}_{\text{stoch}} ,$$

where $\vec{V}_P$ is the particle velocity, U the trapping potential, and $\vec{f}_{\text{stoch}}$ the stochastic thermal forcing. The particle velocity when falling into the trap is of the order of 6 μm/s. The viscous drag force is then of the order of 10^{-13} N. The particle acceleration is of the order of 10 μm s^{-2}. The inertial term is then of the order of 10^{-20} N. At any instant, the velocity of the particle is such that the inertial term (left hand side of the equation) can be neglected: the particle is in the overdamped regime (low Reynolds number). Also the stochastic forcing $\vec{f}_{\text{stoch}}$ is assumed to be much smaller than the trapping force. As a result, at each point of the trajectory shown in Fig. 3(a), the Stokes force equals the trapping force. A spatial integration along the trajectory recovers the trapping potential:

$$U(\rho) = -6\pi\eta a\int_0^{\rho} V_P(\rho')d\rho' .$$

It is plotted in Fig. 3(b) as a function of the position of the center of mass of the particle relative to the center of the trap. The symmetric of this curve with respect to the origin is also plotted for visual convenience. The depth of the potential is $250k_BT$ for an output laser power of 150 mW, consistent with our previous estimate. This value justifies *a posteriori* neglecting the stochastic forcing. Measuring the potential profile for higher output laser power is not possible because of the finite video sampling rate, 30 Hz: a stronger trap pulls the particle faster, and decreases the experimental resolution on the particle trajectory. We thus assume that the potential depth scales linearly with the output laser power. This is confirmed by the linear dependence of the critical velocity V_C on the output power (Fig. 2).

Heating effects are discussed in Appendix A and are shown to be negligible.

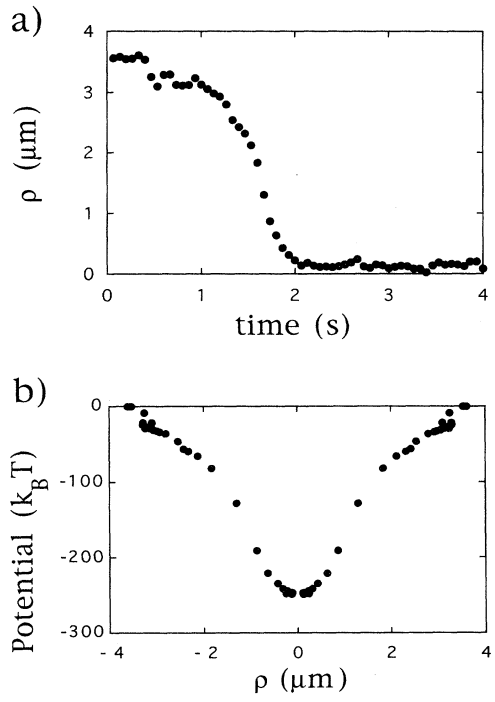

FIG. 3. (a) Time series of the horizontal displacement of a particle falling into the optical trap. The trap is fixed at the origin. Output laser power 150 mW. (b) Trapping potential in units of k_BT for a 2 μm diameter polystyrene sphere. The X axis represents the relative horizontal distance between the particle's center of mass and the beam focal point. Output laser power 150 mW. Laser power at the entrance of the cell 10 mW.

III. OPTICAL TRAP MOVING ON A CIRCULAR PATH

We now move the beam along a circle of diameter 12.4 μm, as shown in Fig. 4. We first describe the experimental setup and the three observed regimes for the particle motion.

A. Experimental setup

Two mirrors $M1$ and $M2$ are mounted on galvanometers [15] oscillating around two perpendicular axes (Fig. 5). This moves the trap in the XY plane transverse to the optical axis. Two telescopes $T1$ and $T2$ allow the beam to pivot about the back iris diaphragm of the microscope objective as the mirrors oscillate (thus preserving the Gaussian beam profile) [16]. The mirrors are synchronously driven by a sine wave signal from a function gen-

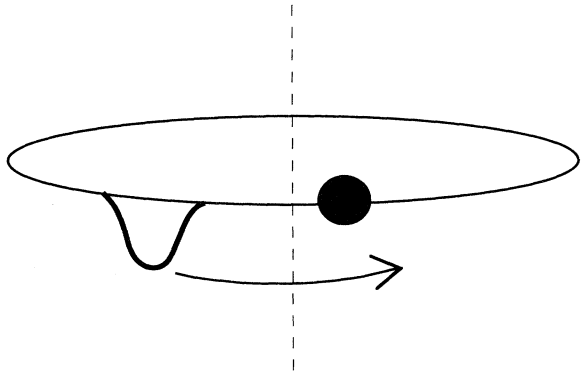

FIG. 4. Rotation of the optical trap along a circle of diameter 12.4 μm.

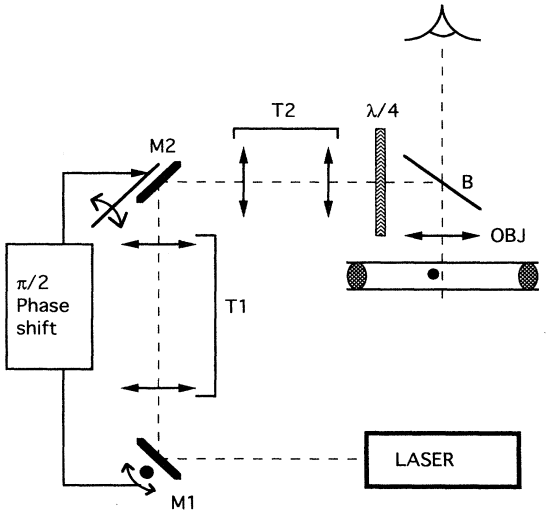

FIG. 5. The beam splitter (B) introduces the infrared laser beam into the microscope's optical path. The microscope objective (OBJ) focuses the beam to a focal point, creating an optical trap. Two mirrors ($M1, M2$) oscillate around two perpendicular axes. A $\pi/2$ phase shift is applied between the two oscillators. The beam focal point moves along a circle. Two telescopes ($T1, T2$) pivot the beam about the back iris diaphragm of the objective (OBJ). The beam is circularly polarized, using a quarter wave plate ($\lambda/4$).

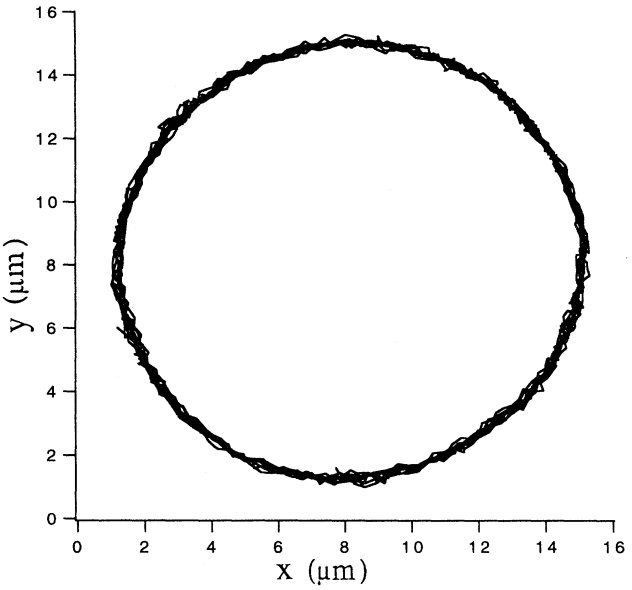

FIG. 6. Trajectory of the particle's center of mass. Recording time 60 s. Trap rotation frequency 14 Hz. Output laser power 700 mW.

erator [17]. A $\pi/2$ phase shift between the mirror oscillations results in a circular motion for the beam in the XY plane. The rotation frequency is the control parameter, which can reach up to 1 kHz. In order to keep the beam intensity constant along the trajectory, circular polarization is used. This is achieved using a quarter wave plate ($\lambda/4$). The potential affecting the particle in the plane transverse to the beam axis is then a symmetric, well shaped potential, rotating around a circle of diameter 12.4 μm (Fig. 4).

B. Particle dynamics

Let us denote the trap rotation frequency by ν_T. The particle trajectory is recorded using the image analysis described in Sec. II A. A typical trajectory is shown in Fig. 6. The particle radial excursions are small compared to the circle diameter ($<3\%$) and to the particle diameter ($<20\%$). We thus approximate the particle motion to be one dimensional and confined to the circle. From the X-Y coordinates of the particle, we extract the particle angular displacement as a function of time. The time series for different trap frequencies are shown in Fig. 7(a). The *mean* angular displacement of the particle is shown in Fig. 7(b). The average is done on periods of the order of 400 s. Fitting the curves by straight lines going through the origin, a well defined mean angular frequency ν_P is measured. It is plotted in Fig. 8 on a logarithmic scale as a function of ν_T for different output laser powers. Each curve presents three distinct regimes: a phase-locked regime where the particle rotates synchronously

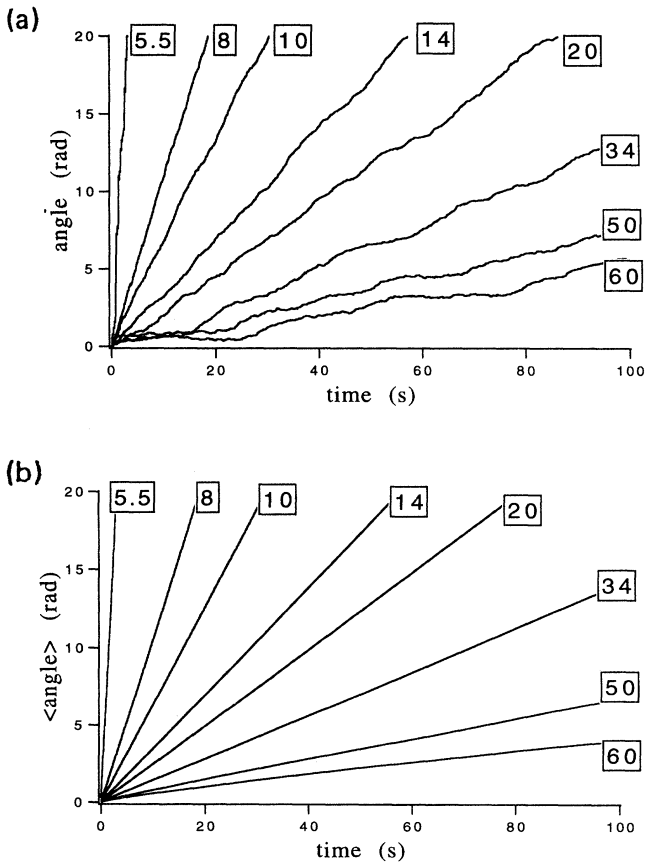

FIG. 7. (a) Time series of the particle's angular displacement for trap rotation frequencies 5.5, 8, 10, 14, 20, 34, 50, and 60 Hz. Output laser power 700 mW. (b) Mean angular displacement of the particle as a function of time. Average over periods of 400 s.

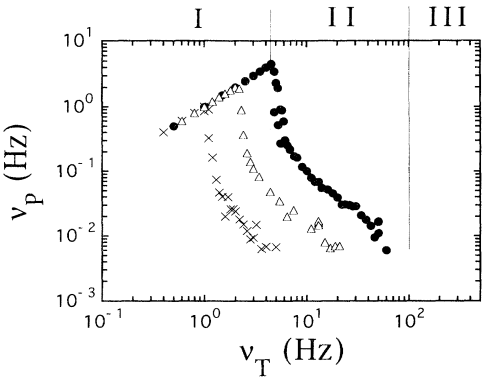

FIG. 8. The particle's mean angular frequency ν_P as a function of the trap angular frequency ν_T. The output laser power is 700 mW (circles), 300 mW (triangles), and 150 mW (crosses). The three regimes are indicated above the graph for an output laser power of 700 mW (circles).

with the trap; a phase-slip regime starting first with a very sharp decrease of ν_P followed by the power law $\nu_P \propto \nu_T^{-1}$; and finally a third regime where the particle's motion along the circle is diffusive, the mean angular frequency ν_P is zero and is not plotted in Fig. 8. These three regimes are delimited by straight vertical lines in Fig. 8 for an output power of 700 mW (circles). In Sec. IV, by rescaling the two frequency axes, we show that all the curves fall onto a single universal function.

Let us now describe in more detail the curve corresponding to a potential depth of $1250 k_B T$ (output laser power 700 mW, circles in Fig. 8). For ν_T smaller than 5 Hz (regime I), the particle is trapped and follows the tweezer. For ν_T between 5 and 70 Hz (regime II) the particle escapes but still rotates around the circle; a mean drift is measured. For ν_T above 70 Hz (regime III), no net angular motion is observed and the particle diffuses freely along the circle: the mean angular frequency is zero. We describe these regimes by comparing the three forces present in this problem. The trapping force has a maximum value of a few piconewtons. The Stokes force is proportional to the particle velocity V_P and opposes any particle motion. The stochastic force is random in time and averages out to zero on a Smoluchowski time scale of the order of 10^{-6} s. A more meaningful measure of it is the average thermal energy $k_B T$.

C. Regime I: Phase-locked regime

At low velocity ($\nu_T \leq 5$ Hz), the Stokes force is smaller than the maximum trapping force: the particle is trapped, its angular frequency is ν_T. This is indicated by the power law of exponent 1 in Fig. 8. This phase-locked regime disappears when reaching a trap rotation frequency higher than the critical frequency ν_C, 5 Hz. The critical particle velocity is then $V_C = 2\pi R \nu_C \approx 190\ \mu\text{m s}^{-1}$. It agrees with the value obtained in Sec. II B by translating the stage, keeping the trap fixed in space.

D. Regime II: Phase-slip regime

In this regime the trap is not strong enough to hold the particle, but kicks it regularly at each revolution. Between kicks the particle diffuses, but does not have enough time to diffuse away from the circle before the return of the trap. The particle is swept along the circle with a well defined *mean* angular velocity. Evidently the angular motion is no longer smooth: the fluctuations in the particle angular position increase with the trap rotation frequency [Fig. 7(a)]. The particle mean angular frequency decreases with the trap frequency: the kicking rotor becomes less and less effective.

One notes just above the critical frequency ν_C a sharp decrease of ν_P. In this region, ν_T is small enough that one can observe individual trapping and escape events of the particle from the moving trap. We now show that these events are characteristic of a stochastic process. Figure 9 shows the time series of the particle angular displacement, for ν_T equals 5.5 Hz. When the particle is trapped and entrained by the trap, the trajectory exhibits almost vertical jumps in Fig. 9. The size of the trapped periods is unevenly distributed, and can be as large as a complete rotation of the particle around the circle (2π rad on the ordinate axis). From direct observation on the video screen of the particle and trap motions, a histogram of the residence times τ in the trap is computed and shown in Fig. 10. The error bars represent the statistical uncertainty. The total number of recorded events is 203. The straight line is a fit of an exponential curve to the experimental points, which gives a mean residence time $\langle \tau \rangle$ of 50 ms (1.83 video frames). This exponential distribution of residence times is a signature of a stochastic es-

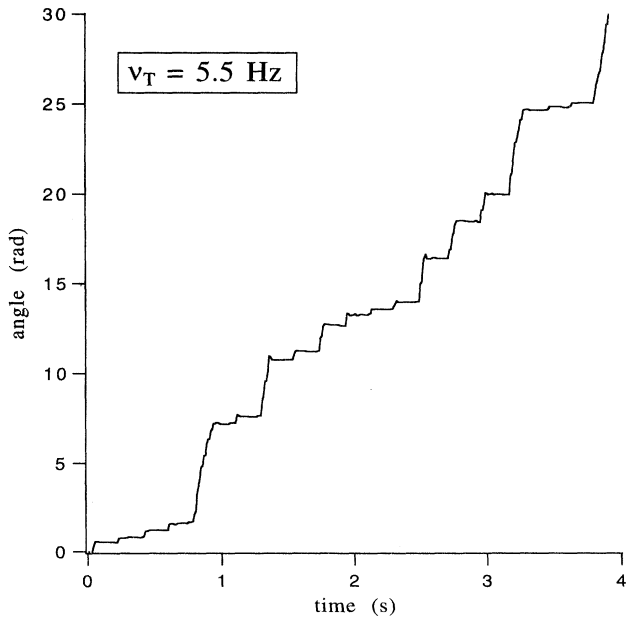

FIG. 9. Time series of the particle angular displacement, trap frequency 5.5 Hz, output laser power 700 mW.

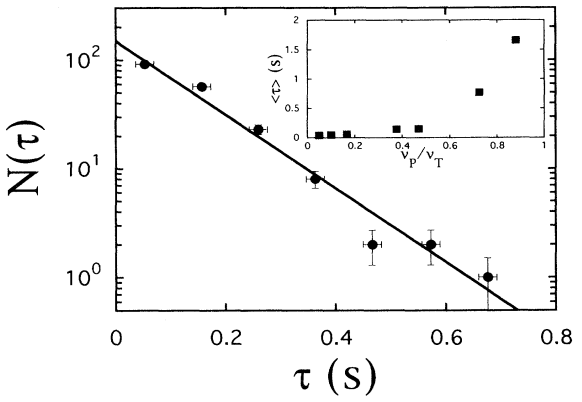

FIG. 10. Histogram of the residence times τ inside the trap, frequency 5.5 Hz, output laser power 700 mW. The vertical error bars represent the statistical uncertainty. The straight line is an exponential fitted to the experimental points. Inset: The particle's mean residence time $\langle\tau\rangle$ in the trap as a function of (ν_P/ν_T). Output laser power 700 mW. Trap rotation frequency ν_T ranging from 4.8 to 5.5 Hz.

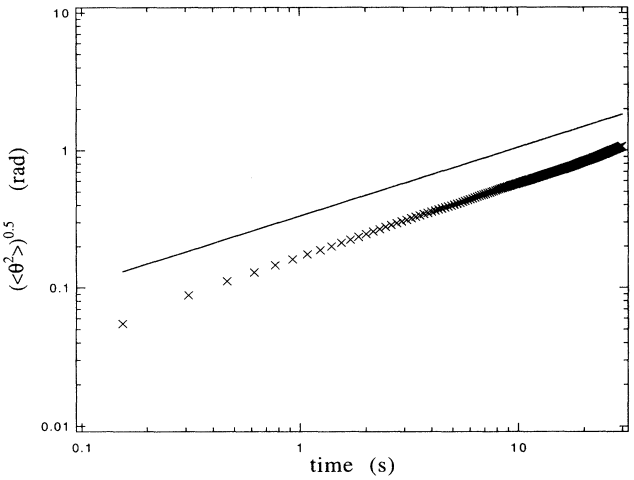

FIG. 11. The root mean square value of the particle angular displacement as a function of time, trap rotation frequency 100 Hz, output laser power 700 mW. The straight line indicates a power law with exponent $\frac{1}{2}$.

cape [14,18]. The mean residence time is a function of the trap frequency. Because of the scatter in the experimental points (see Fig. 8), it is more convenient to look at the dependence of $\langle\tau\rangle$ on the ratio (ν_P/ν_T). This is shown in the inset of Fig. 10. The mean residence time diverges when (ν_P/ν_T) goes to 1 (the particle is locked to the trap rotation and never escapes), and goes to zero when (ν_P/ν_T) goes to zero (the kicking rotor goes too fast to induce a net angular motion of the particle).

E. Regime III: Diffusive regime

Since the kick amplitude decreases with ν_T, it will eventually become smaller than k_BT and thermal effects will dominate the particle's motion, at least on small time scales. This happens for frequencies larger than 70 Hz, for an output laser power of 700 mW. The particle *is still confined in the radial direction* because it always experiences the same side of the optical trap when displaced away from the circle, whereas in the azimuthal direction it experiences both sides of the trapping potential. The particle is essentially free to diffuse along the circle. The particle's mean angular velocity is zero. Figure 11 shows the root mean square value of the angular displacement as a function of time for $\nu_T=100$ Hz. The straight line is a power law of exponent $\frac{1}{2}$, indicating a diffusive motion. Fitting a square root to the experimental points, the angular diffusion constant is $D_\theta=0.008$ rad^2 s^{-1}. The theoretical particle diffusion constant is [19] $D=(k_BT)/(6\pi\eta a)\approx 0.2\ \mu$m^2 s^{-1}. The trap circular trajectory has a radius R of 6.2 μm, thus one estimates $D_\theta\approx D/R^2\approx 0.006$ rad^2 s^{-1}, consistent with the above measurement.

Figure 11 shows that the particle's motion is diffusive over 30 s only. Long time motions are still sensitive to drifts, however small. We used this one dimensional diffusion to build an optical thermal ratchet [20], i.e., a system where the time modulation of a periodic asymmetric potential induces a directed motion of Brownian particles. This configuration could also be used to study the statistics of a one dimensional chain of Brownian particles.

IV. THEORY

We now turn to the response of a Brownian particle to an arbitrarily shaped potential, moving at a velocity V_T [Fig. 12(a)]. The potential and particle motion are one dimensional. The potential has a finite support $[X_a,X_b]$ and is attractive $(U<0)$, such that $U(X_a)=U(X_b)$. In other words, the spatial average of the force is zero. The equation of motion is

$$m\ddot{x}+m\gamma\dot{x}=F(x,t)+f_{\text{stoch}}\ , \tag{1}$$

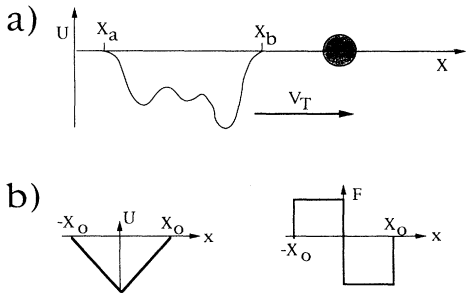

FIG. 12. (a) Particle subjected to the one dimensional motion of an attractive potential, moving at velocity V_T. (b) Triangular potential and corresponding force profile.

where $\gamma=6\pi\eta a/m$ is the damping rate and $F(x,t)$ the force associated with the trapping potential: $F(x,t)=(-\partial/\partial x)U(x,t)$.

The physical parameters are such that the system is in the dissipative limit, i.e., the inertial terms are neglected. We first study the case where the stochastic forcing f_{stoch} is neglected. We then turn to a complete Fokker-Planck treatment of this equation. The opposite limit (conservative case, $\gamma=0$) is treated in Appendix B.

A. Deterministic case

The equation of motion is $m\gamma\dot{x}=F(x,t)=F(x-V_T t)$. The potential, moving along the x axis with a velocity V_T, induces a displacement Δx of the particle during a time Δt. Before and after, the particle is at rest. In the referential frame where the potential is fixed, the new position variable is $y=x-V_T t$. To the potential support $[X_a,X_b]$ corresponds $[Y_a,Y_b]$. The equation of motion is $dy=dt\{[F(y)/m\gamma]-V_T\}$ and the particle total displacement

$$\Delta x=\Delta y+V_T\Delta t=\int_{Y_b}^{Y_a}\left[1+\frac{V_T}{[F(y)/m\gamma]-V_T}\right]dy\ ,$$

or

$$\Delta x=\int_{Y_a}^{Y_b}\frac{F(y)}{m\gamma V_T-F(y)}dy\ . \tag{2}$$

Note that the integration limits in the first integral go from Y_b to Y_a, the order in which the particle experiences the trap.

The period over which the potential produces a motion is

$$\Delta t=\int_{Y_a}^{Y_b}\left[V_T-\frac{F(y)}{m\gamma}\right]^{-1}dy\ . \tag{3}$$

The particle displacement diverges (the particle is trapped) if there is a y such that $F(y)=m\gamma V_T$. Defining F as the maximum value of $F(y)$, the ratio $F/m\gamma$ is the critical trap velocity for escape (maximum velocity for trapping). We now study the large velocity case ($m\gamma V_T>F$), where the particle always escapes.

Let us first show that Δx is positive. In other words, the particle is always displaced in the direction of the moving potential, regardless of the potential shape. Note that we obtain the opposite result in the conservative case (Appendix B). One can check that

$$\Delta x=\int_{Y_a}^{Y_b}\frac{F(y)}{m\gamma V_T-F(y)}dy>\frac{1}{m\gamma V_T}\int_{Y_a}^{Y_b}F(y)dy\ ,$$

whatever the sign of $F(y)$. As $\int_{Y_a}^{Y_b}F(y)dy=0$, the particle displacement is always positive.

The asymptotic behavior is obtained by expanding Eqs. (2) and (3) as a function of the small parameter $F(y)/m\gamma V_T$. This yields

$$\Delta x\approx(1/V_T^2)\int_{Y_a}^{Y_b}[F(y)m\gamma]^2dy$$

and $\Delta t\approx(1/V_T)\int_{Y_a}^{Y_b}dy$. We derive in Appendix C the relation between Δx, Δt, and the particle angular frequency ν_P along the circle. In this limit, $\Delta x\propto V_T^{-2}$ and thus $\nu_P\propto\nu_T^{-1}$, in agreement with the asymptotic power law shown in Fig. 8.

We now turn to a specific potential shape. We approximate the bell-shaped potential in Fig. 3(b) by the triangular symmetric potential shown in Fig. 12(b). It is defined by its width $2X_0$ and its slope F. We associate with F a critical velocity for escape $V_C=F/m\gamma$ and a critical frequency $\nu_C=(V_C/2\pi R)$ on a circle of radius R. ν_C is directly proportional to the output laser power (Fig. 2). It is a known parameter. On the other hand, the potential half width X_0 is a free parameter, such that the triangular potential shown in Fig. 12(b) is equivalent to the optical trap. The two potentials are said to be equivalent when having identical values of $\int_{Y_a}^{Y_b}[F(y)/m\gamma]^2dy$. They then induce the identical particle's rotation frequency ν_P at high enough trap rotation frequency ν_T (Appendix C).

From the potential profile in Fig. 3(b) we integrate numerically the square of the force to find $\int_{Y_a}^{Y_b}[F(y)/m\gamma]^2dy\approx 1060\ \mu\text{m}^3\,\text{s}^{-2}$. The maximum value of the force being $6\pi\eta a V_C\approx 0.54$ pN, the value of X_0 such that a triangle potential is equivalent to the experimental one is of the order of $0.6\ \mu$m.

We now estimate the particle angular frequency for this triangular potential. From Eqs. (2) and (3), $\Delta x=2X_0V_C^2/(V_T^2-V_C^2)$ and $\Delta t=2X_0V_T/(V_T^2-V_C^2)$. From Appendix C, the particle angular frequency is

$$\frac{\nu_P}{\nu_C}=\left[\frac{X_0}{\pi R}\right]\left[\frac{(\nu_T/\nu_C)}{(\nu_T/\nu_C)^2-1}\right]\left[1+\frac{(X_0/\pi R)}{(\nu_T/\nu_C)^2-1}\right]^{-1}\ . \tag{4}$$

(ν_P/ν_C) is a universal function of the rescaled trap rotation frequency (ν_T/ν_C), as shown in Fig. 13. The solid line is computed from Eq. (4) for $X_0=0.6\ \mu$m. The complete agreement shows that thermal noise can be neglected, at least for the *mean* particle angular frequency. It is surprising given the stochastic character of the actual trajectories (see Fig. 9). It is not surprising since the po-

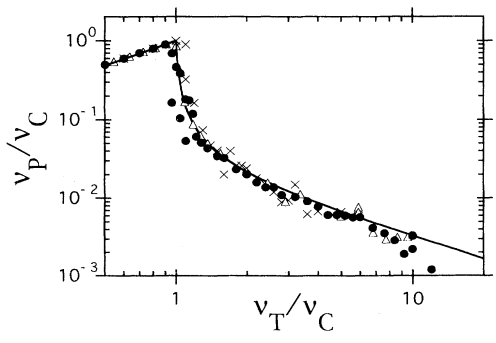

FIG. 13. The nondimensional ratio (ν_P/ν_C) as a function of (ν_T/ν_C). The output laser power is 700 mW (circles), 300 mW (triangles) and 150 mW (crosses). The solid line is computed from Eq. (4), $X_0=0.6\ \mu$m.

tential depth is larger than $250k_BT$ for an output laser power of 150 mW. Under these conditions, the first moment of a trajectory, even stochastic, is still deterministic.

In this deterministic model, the residence time for the particle in the trap is fixed at a constant Δt. In the experiment, the residence time is distributed on an exponential, characteristic of a stochastic process (Figs. 9 and 10). The first moment of the distribution, the mean value $\langle\tau\rangle$, is plotted in the inset of Fig. 10. We compute in our deterministic model Δt as a function of (ν_P/ν_T) from Eqs. (3) and (4). The result is shown in the inset of Fig. 16 for $X_0=0.6$ μm, and agrees with $\langle\tau\rangle$. Again, noise is negligible.

As a final test of the deterministic model, we have studied the effect on ν_P of the potential depth (output power of the laser) for a given trap rotation frequency. Results are shown in Fig. 14(a) for ν_T of 2, 5, and 10 Hz. To an output power we associate a critical frequency ν_C from Fig. 2. In Fig. 14(b) we show that by rescaling by ν_T, the results fall onto a universal curve (solid line, $X_0=0.6$ μm), which can be derived from Eq. (4).

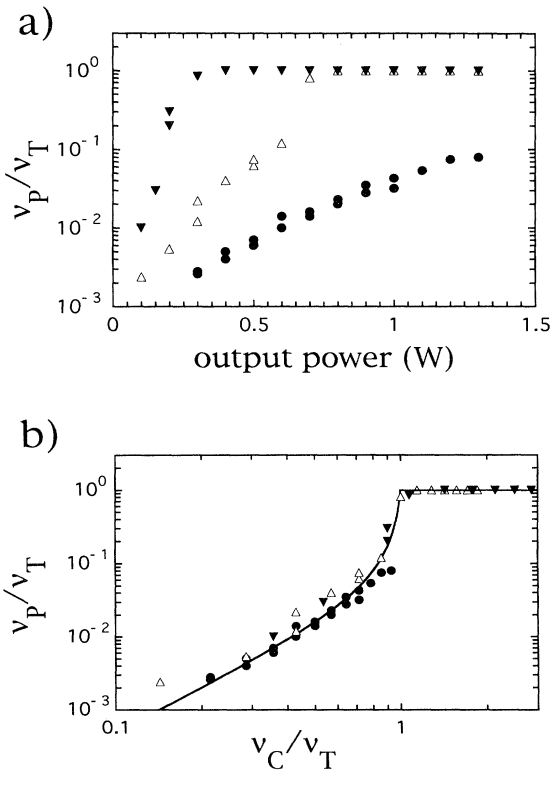

FIG. 14. (a) The ratio (ν_P/ν_T) as a function of the output laser power. The trap rotation frequency is 2 Hz (filled triangles), 5 Hz (open triangles), and 10 Hz (circles). (b) The ratio (ν_P/ν_T) as a function of (ν_C/ν_T). Trap rotation frequency 2 Hz (filled triangles), 5 Hz (open triangles), and 10 Hz (circles), output laser power ranging from 100 mW to 1.3 W. The solid line is computed from Eq. (4), $X_0=0.6$ μm.

B. Fokker-Planck approach

We now study the effect of temperature. In the referential frame where the potential is fixed, the Fokker-Planck equation [21,22] corresponding to the Langevin equation of Sec. IV A is written

$$\frac{\partial}{\partial t}W(y,t)=-\frac{\partial}{\partial y}J(y,t)\ , \tag{5}$$

where $W(y,t)$ is the probability density of the particle and the probability current $J(y,t)$ is

$$J(y,t)=\frac{W(y,t)}{m\gamma}[F(y)-m\gamma V_T]-\frac{k_BT}{m\gamma}\frac{\partial}{\partial y}W(y,t)\ . \tag{6}$$

As we are looking for stationary solutions for $W(y,t)$ we set to zero the left hand side of Eq. (5); the current is then a constant $[J(y,t)=J]$. The steady state solution is then also a general solution of Eq. (6):

$$W(y)=\left[C-\frac{Jm\gamma}{k_BT}\int_0^y dy'\exp\left[\frac{U(y')+m\gamma V_Ty'}{k_BT}\right]\right]\times\exp\left[-\frac{U(y)+m\gamma V_Ty}{k_BT}\right].$$

Because the trap motion occurs on a circle of radius R, we set the stationary probability density $W(y)$ to be periodic of period $L=2\pi R$. This implies a relation between the particle current J and the undefined constant C. Inserting this relation back into the expression of $W(y)$ leads to

$$W(y)=\frac{Jm\gamma}{k_BT}\left[1-\exp\left[\frac{m\gamma V_TL}{k_BT}\right]\right]^{-1}\times\int_0^L dy'\exp\left[\frac{U(y+y')-U(y)+m\gamma V_Ty'}{k_BT}\right].$$

The particle current J is now obtained by demanding that the particle probability density $W(y)$ be normalized to 1. This involves a second integral of $W(y)$ over the circle perimeter L and yields

$$\frac{k_BT}{Jm\gamma}\left[1-\exp\left[\frac{m\gamma V_TL}{k_BT}\right]\right]=\int_0^L dy\int_0^L dy'\exp\left[\frac{U(y+y')-U(y)+m\gamma V_Ty'}{k_BT}\right]. \tag{7}$$

The above equation relates the particle current J to the physical parameters of our system: the potential $U(y)$, the trap velocity V_T, and the temperature T. The mean value of the particle velocity in the referential frame where the potential is fixed is simply $V_P=JL$. In the absence of potential, this mean velocity would be $V_P=-V_T$. The presence of a force, however, delays the motion of the particle, and induces a positive drift $\Delta V=V_P+V_T$, whatever the referential frame. Since the motion takes place on a circle of radius R, the *mean* an-

gular frequency of the particle is given by $\nu_P = \Delta V / 2\pi R$.

We show in Appendix D that Eq. (7) implies that ν_P scales asymptotically as ν_T^{-1}. The resulting expression for ν_P is independent of the temperature, and is identical to the one derived in Appendix C within the deterministic model of Sec. IV A.

We now approximate the trapping potential to be triangular as shown in Fig. 12(b). For such a potential, one can solve analytically for the probability current J and the particle rotation frequency ν_P. The complete expressions are given in Appendix E.

The value of (ν_P/ν_C), as computed in Appendix E, is shown in Fig. 15 as a function of (ν_T/ν_C) for different temperatures. The deterministic curve ($T=0$ K, solid line) is computed from Eq. (4). The room temperature ($T=300$ K) curve is almost indistinguishable from the deterministic one: we show in the inset of Fig. 15 the deviation of the ($T=300$ K) solution from the ($T=0$ K) solution, close to the transition from a phase-locked regime to a phase-slip regime. It is close to this transition that the effect of noise is the strongest: the small thermal fluctuation can make the particle escape from the trap where it was barely held. The almost complete agreement between the two curves explains why the deterministic model is so powerful in describing the experimental behaviors: the potential depth is so large compared to the noise ($250 k_B T$ for the minimum output laser power of 150 mW), that the temperature can be set to zero when computing the particle's rotation frequency.

As shown in Appendix E, the end result for ν_P depends only on $m\gamma V_T/k_B T$ and $m\gamma V_C/k_B T$. Thus, reducing the potential depth (and therefore V_C) is equivalent to increasing the temperature. Curves at higher temperatures ($T=3000$, 10 000, and 30 000 K) are also plotted in Fig. 15 to illustrate the effect of thermal noise on ν_P. ν_P always decreases when T increases: the kicking rotor becomes less efficient when more noisy. Also, as ν_T goes to infinity, all curves collapse on the asymptotic scaling discussed in Appendixes C and D. Finally, the trap rotation frequency at which the particle escapes from the trap also decreases when T increases: thermal fluctuation favors the escape of a Brownian particle from a potential trap, moving or not.

We now estimate the mean residence time $\langle \tau \rangle$ of the particle inside the moving trap. The probability of finding the particle inside the trap is equal to the integral of $W(y)$ between Y_a and Y_b: $\int_{Y_a}^{Y_b} W(y)dy$. This is also equal to the fraction of time the particle is trapped. Over one cycle, the particle is trapped during a time $\langle \tau \rangle$ and the trap comes back under it in a time $(L-2X_0)/V_T$. The fraction of time the particle is trapped is thus

$$\frac{\langle \tau \rangle}{\langle \tau \rangle + \dfrac{(L-2X_0)}{V_T}} = \int_{Y_a}^{Y_b} W(y)dy \ ,$$

which yields

$$\langle \tau \rangle = \frac{\displaystyle\int_{Y_a}^{Y_b} W(y)dy}{1-\displaystyle\int_{Y_a}^{Y_b} W(y)dy} \left[\frac{L-2X_0}{V_T} \right] . \tag{8}$$

This expression is computed using Eq. (E1). It is plotted in Fig. 16 as a function of (ν_T/ν_C) for $X_0 = 0.6$ μm,

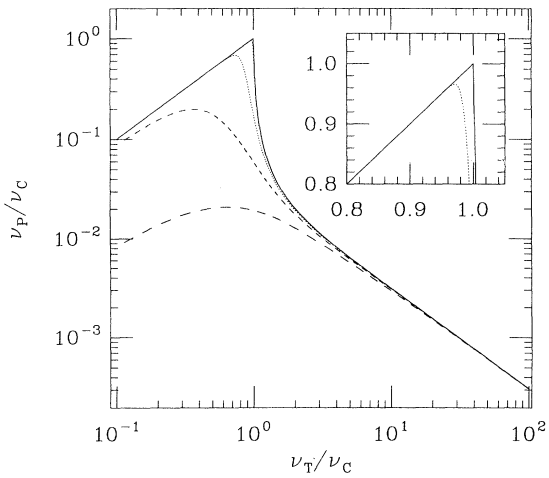

FIG. 15. The ratio (ν_P/ν_C) as a function of (ν_T/ν_C), for different temperatures. The solid line ($T=0$ K) is from Eq. (4). The dashed lines are computed from Appendix E, temperatures $T=300$, 3000, 10 000, and 30 000 K. The higher T, the farther the dashed curves from the solid one. The parameters are $X_0 = 0.6$ μm, $V_C = 100$ μm s^{-1}, $R = 6.2$ μm. The inset is a blow-up of the ($T=0$ K) and ($T=300$ K) curves close to the transition from the phase-locked to the phase-slip regime ($\nu_T/\nu_C = 1$).

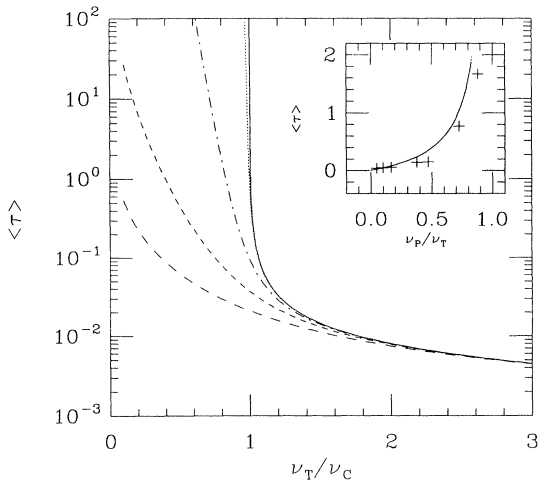

FIG. 16. The mean residence time $\langle \tau \rangle$ of the particle in the moving trap as a function of (ν_T/ν_C). The solid line ($T=0$ K) is computed from Eq. (3), the dashed lines are computed from Eq. (8) for temperatures $T=300$, 3000, 10 000, and 30 000 K. The parameters are $X_0 = 0.6$ μm, $V_C = 100$ μm s^{-1}, $R = 6.2$ μm. The inset reproduces the inset from Fig. 10, with the ($T=0$ K, solid line) and ($T=300$ K, dashed line) theoretical values for $\langle \tau \rangle$.

$V_C = 100\ \mu m\, s^{-1}$, $R = 6.2\ \mu m$, and for temperatures $T = 300$, 3000, 10 000, and 30 000 K. Again the ($T = 300$ K) curve is almost indistinguishable from the deterministic ($T = 0$ K) curve from Eq. (4). Note that $\langle \tau \rangle$ diverges as (ν_T / ν_C) approaches 1 in the deterministic model. For any nonzero temperature, $\langle \tau \rangle$ is always finite and smaller than the Kramers time [23] (mean residence time of the particle in a fixed trap). As the temperature or the trap rotation frequency increases, $\langle \tau \rangle$ decreases. It reaches for large ν_T the deterministic limit: $\langle \tau \rangle \approx \Delta t = (1/\nu_T)(X_0/\pi R)$, as illustrated by the collapse of all the curves for large ν_T.

Theoretical considerations similar to the ones presented in this section have been studied in the context of reversible computation [24].

V. CONCLUSION

For a given output power (given trapping force), we observe three regimes for the response of a Brownian particle (2 μm diameter polystyrene sphere in water) to an optical trap rotating in a circle. These three regimes are determined by the trap rotation frequency ν_T.

When the drag force is smaller than the maximum trapping force, the particle follows the trap up to a critical frequency ν_C ($\nu_C = 5$ Hz for an output power of 700 mW). For larger drag forces the particle escapes from the trap. Nevertheless a net *mean* angular velocity ν_P is still measured when the kick amplitudes are larger than $k_B T$. It scales asymptotically as the inverse of the trap frequency. In the thermal noise dominated regime ($\nu_T > 70$ Hz for an output power of 700 mW), we observe the one dimensional diffusion of the particle along the circle. These three regimes are characteristic of a noisy asynchronous rotor: to a phase-locked regime succeeds a phase-slip regime, and then a diffusive regime.

We describe the experimental observations within a simple deterministic ($T = 0$ K) model. We show that the dependence of (ν_P / ν_C) on (ν_T / ν_C) for different output powers falls onto a universal curve. Solving the Fokker-Planck equation (which takes into account the effect of a nonzero temperature), we justify the ($T = 0$ K) model: the potential depth is always much larger than the thermal noise $k_B T$. The first moments are deterministic, even though the trajectories themselves are noisy.

ACKNOWLEDGMENTS

It is a pleasure to thank Laurent Bourdieu, Peter Kaplan, and Albrecht Ott for their help in designing and building the experimental setup. We thank Marcelo O. Magnasco and Armand Ajdari for enlightening discussions. We thank R. Landauer for bringing Ref. [24] to our attention.

APPENDIX A: HEATING EFFECTS

We now discuss thermal gradients inside the cell. P_0 is the laser power in the cell ($P_0 = 50$ mW at most, see Sec. II B) and χ_0 the thermal conductivity of water ($\chi_0 = 0.6$ W m^{-1} K^{-1}). Polystyrene and water have approximately the same value for the absorption length l_0 in the infrared ($l_0 = 10$ cm). The power absorbed by the sphere of radius a is $P_{abs} \approx P_0 (a/l_0)$, of the order of 10^{-6} W. In the steady state, this power is dissipated in the surroundings by the heat current: $\vec{J}_Q = -\chi_0 \vec{\nabla} T$, where T is the temperature field in water. Because of spherical symmetry, T is a function only of the radial coordinate r, and so the heat current is radial and equal in magnitude to $\chi_0 [dT(r)/dr]$. The heat flux across a spherical shell of radius r enclosing the polystyrene sphere gives the absorbed power:

$$P_{abs} = \oiint \vec{J}_Q \cdot \vec{n} = 4\pi r^2 \chi_0 \frac{dT(r)}{dr} .$$

From spatially integrating this equation and fixing the temperature far away from the sphere to be equal to the room temperature, the temperature rise at the surface of the polystyrene sphere is $\Delta T = P_{abs}/4\pi a \chi_0 \approx 10^{-1}$ K.

The relative change in temperature ($\Delta T / T$) is thus of order 0.03%. Taking the thickness of the cell to be 50 μm, one can scale the above analysis to check that the total temperature rise is no more than 5 K ($\Delta T / T = 1.5\%$).

APPENDIX B: CONSERVATIVE CASE, $\gamma = 0$

In the conservative case, the equation of motion reads $m\ddot{x} = F(x,t)$. The total energy of the system is conserved. In the referential frame where the potential is fixed, this conservation law reads $\frac{1}{2} m \dot{y}^2 + U(y) = \frac{1}{2} m V_T^2$, or

$$dt = -\frac{dy}{\sqrt{V_T^2 - [2U(y)/m]}} .$$

The particle displacement is

$$\begin{aligned} \Delta x &= \Delta y + V_T \Delta t \\ &= \int_{Y_b}^{Y_a} dy \left[1 - \frac{V_T}{\sqrt{V_T^2 - [2U(y)/m]}} \right] \\ &= \int_{Y_a}^{Y_b} dy \left[\frac{1}{\sqrt{1 - [2U(y)/mV_T^2]}} - 1 \right] . \end{aligned}$$

It is worth noting that since $U(y) < 0$ for all y, so is Δx, whatever the potential shape. This somehow counterintuitive result means that the particle displacement is in the direction opposite to the trap motion. Also, for large enough trap velocities, $|2U(y)/mV_T^2| \ll 1$ and the above equation can be Taylor expanded as $\Delta x \approx [\int_{Y_a}^{Y_b} U(y) dy](1/mV_T^2)$.

Here again the particle displacement scales asymptotically as the inverse square of the trap velocity. If the motion occurs in a circle, the particle rotation frequency will scale as the inverse of the trap rotation frequency. The overall rotation of the particle will, however, be in the direction opposite to the trap rotation.

APPENDIX C: MOTION IN A CIRCLE

On a line, the particle displacement Δx [Eq. (2)] induced by the moving potential occurs during a time Δt [Eq. (3)]. On a circle of radius R (6.2 μm in our experiment), the particle angular displacement is $\Delta\theta = (\Delta x / R)$. Once the particle escapes from the trap, it is caught again

after the trap comes back: this takes an extra time

$$\frac{2\pi R-2X_0}{V_T}=\frac{1}{\nu_T}\left[1-\frac{X_0}{\pi R}\right],$$

where $2X_0$ is the total width of the potential ($2X_0=Y_b-Y_a$). The particle angular frequency along the circle is then

$$\nu_p=\frac{\Delta x}{2\pi R}\left[\Delta t+\frac{1}{\nu_T}\left[1-\frac{X_0}{\pi R}\right]\right]^{-1}. \tag{C1}$$

In the large trap velocity regime, Eq. (3) yields $\Delta t\approx(1/V_T)\int_{Y_a}^{Y_b}dy\approx(1/\nu_T)(X_0/\pi R)$. Equation (C1) reduces then to

$$\nu_p\approx(\Delta x/2\pi R)\nu_T .$$

From Eq. (2), the particle's rotation frequency is then

$$\nu_p\approx\frac{1}{\nu_T}\frac{1}{(2\pi R)^3}\int_{Y_a}^{Y_b}\left[\frac{F(y)}{m\gamma}\right]^2dy . \tag{C2}$$

The particle's rotation frequency scales as the inverse of the trap rotation frequency. This is the asymptotic power law shown in Fig. 8 for each curve, and in Fig. 13 when rescaling the frequencies by the critical frequency ν_C.

APPENDIX D: ASYMPTOTIC SCALING OF THE FOKKER-PLANCK EQUATION

We show here that the asymptotic scaling of ν_P for large ν_T predicted by the Fokker-Planck approach is identical to the deterministic one [Eq. (C2)]. We first assume that $m\gamma V_T\gg F(y)$ for all y in the finite support of the potential, and rewrite Eq. (7) as

$$\frac{k_BT}{Jm\gamma}\left[1-\exp\left[\frac{m\gamma V_TL}{k_BT}\right]\right]=\int_0^Ldy\int_0^Ldy'\exp\left[\frac{m\gamma V_Ty'}{k_BT}\left[1+\frac{U(y+y')-U(y)}{m\gamma V_Ty'}\right]\right].$$

In this expression, $[U(y+y')-U(y)]/m\gamma V_Ty'$ is a small parameter that we approximate by $-F(y)/m\gamma V_T$. Expanding the exponential as a function of this small parameter and integrating over y', we obtain

$$\frac{1}{J}\approx-\frac{1}{V_T}\int_0^Ldy\left[1+\frac{F(y)}{m\gamma V_T}+\left[\frac{F(y)}{m\gamma V_T}\right]^2\right].$$

Since $\int_0^Ldy\,F(y)=0$, the particle current is then given by

$$J\approx-\frac{V_T}{L}\left[1-\int_0^L\left[\frac{F(y)}{m\gamma V_T}\right]^2dy\right].$$

The particle's mean rotation frequency is $\nu_P=\Delta V/2\pi R=(JL+V_T)/2\pi R$. Within the above approximation, it reduces to

$$\nu_P\approx\frac{1}{\nu_T}\frac{1}{(2\pi R)^3}\int_{Y_a}^{Y_b}\left[\frac{F(y)}{m\gamma}\right]^2dy . \tag{D1}$$

This expression is identical to Eq. (C2): in the asymptotic limit of infinite trap velocity the Fokker-Planck equation and the deterministic Langevin equation give the same result for the mean particle's rotation frequency ν_P. It is independent of temperature and scales as ν_T^{-1}.

APPENDIX E: FOKKER-PLANCK RESULTS FOR A TRIANGULAR POTENTIAL

The potential shape shown in Fig. 12(b) is assumed to be centered at $L/2$, where L is the circle perimeter ($L=2\pi R$). We define the following constants: $\alpha=m\gamma V_T/k_BT$ is a measure of the trap velocity and $s=m\gamma V_C/k_BT$ a measure of the trapping force. The integral $I=\int_0^L\exp[U(y)+\alpha y]dy$ is given explicitly as

$$I=\frac{e^{\alpha Y_a}-1}{\alpha}+\frac{e^{(\alpha-s)(L/2)}e^{+sY_a}-e^{\alpha Y_a}}{\alpha-s}+\frac{e^{\alpha Y_b}-e^{-sY_b}e^{(\alpha+s)(L/2)}}{\alpha+s}+\frac{e^{\alpha L}-e^{\alpha Y_b}}{\alpha}.$$

We also define $I_n=I[e^{-\alpha L}/(1-e^{-\alpha L})]$. With these notations, the particle's rotation frequency is given by $\nu_P=(JL+V_T)/2\pi R$, where the probability current J is

$$J=\frac{-k_BT}{m\gamma}\frac{1}{[P_1+P_2+P_3+P_4]} .$$

The four terms in the denominator are

$$P_1=\frac{Y_a}{\alpha}+\frac{1-e^{-\alpha Y_a}}{\alpha}\left[I_n-\frac{1}{\alpha}\right],$$

$$P_2=\frac{X_0}{\alpha-s}+\left[\frac{e^{(s-\alpha)X_0}-1}{s-\alpha}\right]\times\left[\frac{s}{\alpha(s-\alpha)}+e^{-\alpha Y_a}\left[I_n-\frac{1}{\alpha}\right]\right],$$

$$P_3=\frac{X_0}{\alpha+s}+\left[\frac{e^{(s+\alpha)X_0}-1}{s+\alpha}\right]\times\left[\frac{s}{\alpha(s+\alpha)}+e^{\alpha Y_a}\left[I_n-\frac{1}{\alpha}\right]\right],$$

$$P_4=\frac{Y_a}{\alpha}+\frac{e^{\alpha Y_a}-1}{\alpha}\left[I_n-\frac{1}{\alpha}\right].$$

P_1 is written formally as

$$P_1=\frac{1}{1-e^{\alpha L}}\left\{\int_0^{Y_a}dy\int_0^{L}\exp\left[\frac{U(y+y')-U(y)}{k_BT}\right]e^{-\alpha y'}\right\},$$

or

$$P_1=\left[\frac{k_BT}{-Jm\gamma}\right]\int_0^{Y_a}W(y)dy\ .$$

The terms P_2, P_3, and P_4 are obtained in a similar way by integrating, respectively, from Y_a to $L/2$, from $L/2$ to Y_b, and from Y_b to L. A useful relation for the mean residence time computation is

$$\int_{Y_a}^{Y_b}W(y)dy=(P_2+P_3)\left[\frac{-Jm\gamma}{k_BT}\right]. \tag{E1}$$

[1] A. Ashkin, Phys. Rev. Lett. **24**, 156 (1970).
[2] A. Ashkin, J. M. Dziedic, J. E. Bjorkholm, and S. Chu, Opt. Lett. **11**, 288 (1986).
[3] Bangs Laboratories, Inc., Carmel, IN.
[4] The water was purified by a Millipore ultrapure water system (Millo-RO 10 plus and Milli-Quf plus) from Millipore Corp., Bedford, MA.
[5] $75\times50\times1$ mm^3 precleaned microscope slides from Corning Glass Works, Inc., Corning, NY.
[6] $22\times22\times0.05$ mm^3 coverslips number 0 from Fisher Scientific, Inc., Pittsburgh, PA.
[7] Simco Topgun from Simco, Inc., Hatfield, PA.
[8] Five minute fast epoxy from Devcon Corp., Danvers, MA.
[9] Upright microscope model Axioskop from Carl Zeiss, Inc., Thornwood, NY.
[10] TI-24 CCD camera from NEC Electronics, Inc., Mountainview, CA.
[11] Perceptics PixelBuffer model PTB 425 from Perceptics Corp., Knoxville, TN, used with a MacIIFx computer from Apple Computers, Inc., Cupertino, CA.
[12] Model C-105 from CVI Laser Corp., Albuquerque, NM.
[13] Zeiss Plan-Neofluar 100.
[14] A. J. Simon, Ph.D. thesis, University of Chicago, 1992 (unpublished).
[15] Mirror positioning system model 650× from Cambridge Technology, Inc., Watertown, MA.
[16] K. Svoboda and S. Block, Annu. Rev. Biophys. Biomol. Struct. **23**, 247 (1994).
[17] Synthesizer model 3325B from Hewlett Packard Corp., Sunnyvale, CA.
[18] A. Simon and A. Libchaber, Phys. Rev. Lett. **68**, 3375 (1992).
[19] A. Einstein, Ann. Phys. (N.Y.) **17**, 549 (1905).
[20] L. P. Faucheux, L. S. Bourdieu, P. D. Kaplan, and A. J. Libchaber, Phys. Rev. Lett. **74**, 1504 (1995).
[21] H. Risken, *The Fokker-Planck Equation* (Springer-Verlag, New York, 1989).
[22] N. G. Van Kampen, *Stochastic Processes in Physics and Chemistry*, North-Holland Personal Library (Elsevier Science, Amsterdam, 1981).
[23] H. A. Kramers, Physica (Utrecht) **7**, 284 (1940).
[24] R. Landauer and M. Büttiker, Phys. Scr. **T9**, 155 (1985).

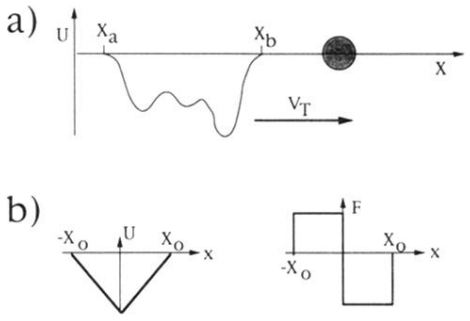

FIG. 12. (a) Particle subjected to the one dimensional motion of an attractive potential, moving at velocity V_T. (b) Triangular potential and corresponding force profile.

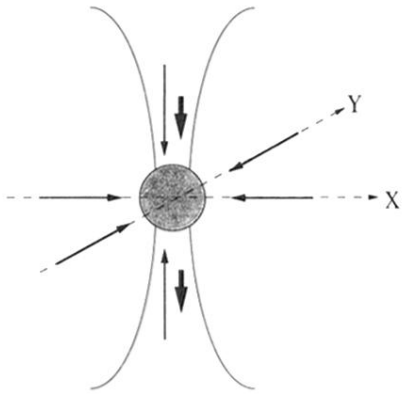

FIG. 1. A 2 μm diameter polystyrene particle trapped near the focal point of a Gaussian laser beam propagating down the vertical axis. The gradient forces are shown on each axis as the thin solid arrows. The radiation pressure is indicated by the thick solid arrows.